ACS Photonics

pubs.acs.org/journal/apchd5

Article

Self-Assembled Nano−Lotus Pod Metasurface for Light Trapping

Nayeun Lee, Reehyang Kim, Ju Young Kim, Jong Beom Ko, Sang-Hee Ko Park, Sang Ouk Kim, Mark L. Brongersma, and Jonghwa Shin*

Cite This: https://doi.org/10.1021/acsphotonics.0c01882

Read Online

ACCESS | Metrics & More | Article Recommendations | Supporting Information

ABSTRACT: Concentration of electromagnetic waves in deep-subwavelength volumes has been widely investigated as a direct way of enhancing light-matter interactions. However, a homogeneous array of subwavelength nanogaps suitable for visible light localization and enhancement is difficult to realize due to the limitations of conventional lithography techniques. Here, a uniform array of ultrasmall plasmonic resonators with precisely controlled nanogaps ("nano−lotus pods") is presented for the visible light confinement and realized without any photo- or beam-based lithography steps. The unit motif of this metasurface with a physical volume of $52 \times 60 \times 40$ nm^3 is designed to resonantly trap visible light into an effective mode volume of $1.57 \times 10^{-5}\lambda_0^3$. Each nano−lotus pod can be considered as a curved metal−insulator−metal waveguide which exposes both of its end faces and thus hot spots with the strongest electric fields on the outermost flat surface. To realize this unique nanostructure, a template-stripping method is employed in conjunction with block copolymer self-assembly and atomic layer deposition which guarantee a homogeneous array over large areas. It is experimentally demonstrated that the proposed metasurface can be used as a highly uniform and flat substrate for surface-enhanced Raman spectroscopy of various analytes, especially a stiff two-dimensional material.

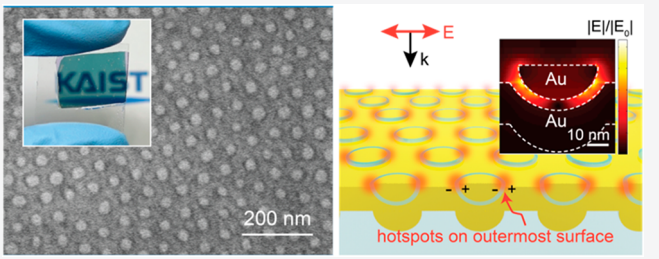

KEYWORDS: *metasurface, mode volume, surface-enhanced Raman spectroscopy, plasmonics, nanogap*

The confinement of light to a nanoscale volume can enhance light-matter interactions by many orders of magnitude.[1−3] So far, many nano-optical structures with local field enhancement have been proposed as a promising route to achieve high performances in applications ranging from molecular sensors to single-quantum emitters,[4−6] as well as to study novel light−matter interactions in low-dimensional materials.[7,8] In particular, it has been demonstrated that surface plasmon-polariton waves in a single metal−insulator−metal (MIM) waveguide (gap-plasmons) can be utilized to squeeze light into a few-nanometer-wide dielectric gap to achieve light−matter interactions with an unprecedented strength.[9] The mode volume, which quantifies how tightly the electric field is confined spatially, is directly linked to the strength of the interaction. For this reason, resonators with tiny gaps have been proposed to achieve small mode volumes ($10^{-5} \sim 10^{-7}\lambda_0^3$)[10−12] and a strong light−matter interaction in the near-infrared wavelength region, as well as in the visible spectrum.[6,10,13−15]

However, there are two substantial hurdles that are preventing widespread adoption of these structures in practical devices. First, on the fabrication side, it is a daunting task to generate precisely controlled few-nanometer gaps uniformly over a large area. Using fabrication techniques such as beam-based lithography and nanosphere lithography, one can achieve horizontally defined nanogaps by bringing two metal structures close to each other.[13,16−19] As the resonance of the nanogap resonators largely depends on the thickness of nanogap, it is important to produce a precisely controlled thickness of nanogaps over the sample area. Also, to make an operational wavelength of such nanogap resonators in the visible wavelengths, the dimension of the metal structure is often required to be in the sub-hundred nanometer regime and, in many cases, designed to be intricately shaped for the best optical performance.[20,21] This makes it challenging both for the conventional lithography methods, including controlling etching and deposition time due to the nanometer resolution required, and for the particle synthesis-based methods due to the requirement of strict homogeneity and asymmetric or complicated structural shapes over a large area.[22] Rather than defining horizontal nanogaps, there has been rich investigation on the fabrication of vertical nanogap resonators by stacking metal particles on top of metal substrate with thin dielectric layers.[23] While it is possible to define nanogaps in a controllable manner, the induced strong electric fields are often embedded inside two metal domains. This leads us to the

Received: December 11, 2020

second hurdle, which lies in the design aspect: in many of the previously proposed structures, the "hot spots" with the highest intensity fields are recessed from the surface, which makes it hard to utilize these hot spots for sensing rigid analytes or large molecules. Also, in some cases, the position of the hot spots is random, contributing to the nonuniformity and batch-to-batch variability of signal enhancement factors, which renders quantitative analysis using these hot spots difficult. Overcoming these hurdles and devising a reliable fabrication process and new structural design that can produce a deterministic, homogeneous array of nanoresonators with exposed hot spots in the visible spectrum would enable the practical use of gap plasmon resonators.

In this work, we propose and realize a homogeneous array of three-dimensional nano−lotus pod resonators, confining visible light within a mode volume of $1.57 \times 10^{-5}\lambda_0^3$ per resonator. The unit structure, with a 30 nm inner diameter and a 5 nm thick dielectric gap, serves as an ultrasmall waveguide-based optical cavity with truly nanoscale confinement in all three dimensions. Through the synergistic combination of MIM waveguide mode and surface plasmon resonance physics, the electric field is tightly confined in the gap between two metal domains. It is possible to engineer the optical properties such as resonance wavelength with the geometrical parameters of the resonators. We designed our nanogap resonator such that it operates in the visible spectral region with the ultrasmall physical size of the resonator structure. Moreover, the resonators were fabricated as a very uniform array over a centimeter-scale area without any lithographic step, by combining block copolymer self-assembly with atomic layer deposition (ALD) and template stripping methods. This extends the pioneering works that combined atomic layer deposition with a template stripping technique to achieve high throughput of the precisely defined metallic nanogap resonators operating in the terahertz and long-wavelength infrared regimes to the visible wavelengths.[24,25] As block copolymers self-assemble into periodic sub-100 nm nanostructures over a large area simply by spin-coating and thermal annealing, orders of magnitude increase in throughput and decrease in cost can be expected over electron or ion beam-based lithographic methods of nanofabrication.[26−28]

Figure 1 presents a schematic of the process flow used to fabricate the nano−lotus pod array. Polystyrene-*b*-poly(methyl methacrylate) (PS-*b*-PMMA) block copolymer that anneals to a hexagonal array of vertical PMMA cylinders was used as the starting template, as previously described.[29] The PMMA region was selectively etched to produce a PS matrix with cylindrical holes having diameters of 30 nm and a height of 80 nm. Upon this template, 15 nm thick gold was deposited by thermal evaporation, and then the PS matrix was lifted off to reveal a hexagonal array of gold nanodots. Afterward, a 5 nm thick Al_2O_3 layer was deposited by ALD, followed by an additional gold layer (20 nm thick, thermal evaporation). Using this method, the ALD-grown Al_2O_3 layer thickness determines the separation between the gold nanodots and the top gold layer, allowing uniform, atomic-level control of the gap size over the entire sample area.

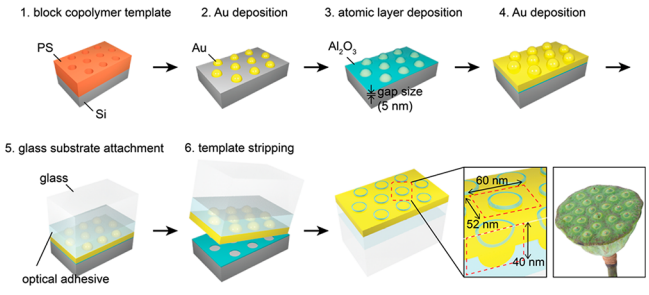

Figure 1. Schematic depiction of the nano−lotus pod structure fabrication process. A block copolymer template was formed on a silicon substrate upon which an atomic layer deposition with template stripping technique was applied. (Inset) A picture of a lotus pod. Credit: Tevarak/istockphoto.com.

For template stripping, an optical adhesive (NOA 61, Norland product) was dropped onto the sample, and a glass substrate was attached on top of the adhesive. After 1 h of UV light treatment in the cross-linker, the adhesive layer was firmly attached to the glass substrate as well as to the gold nanostructures. Due to their weak adhesion to silicon, the gold nanostructures can be easily stripped off from the silicon substrate by lifting the glass. The Al_2O_3 layer located between the gold nanodots is strongly attached to the silicon substrate and remains on the substrate after stripping, as verified by atomic force microscopy (AFM) images (Figure S1 in the Supporting Information). The unit volume of the nano−lotus pod is $52 \times 60 \times 40$ nm^3, which is smaller than the structures in previous reports of template stripping by more than 1 order of magnitude,[30] demonstrating that the template-stripping method can be applied to sub-100 nm scale objects. This procedure is unique in that it allows the fabrication of an optically uniform metasurface of deep-subwavelength three-dimensional nanostructures without the use of any patterned mask or beam-based patterning steps.

The fabricated sample area was more than 1 cm^2 and potentially scalable to 4 in. or larger wafers. Figures 2a and S2 in the Supporting Information show photographs of the fabricated sample. Since its light absorption due to excitation of the gap plasmon resonances is strongest in the red spectral range, the gold nano−lotus pod structure exhibits a distinctive green color. It is noteworthy that the sample appears as a homogeneous semitransparent film, even though individual resonators are strongly scattering, which is only possible if the

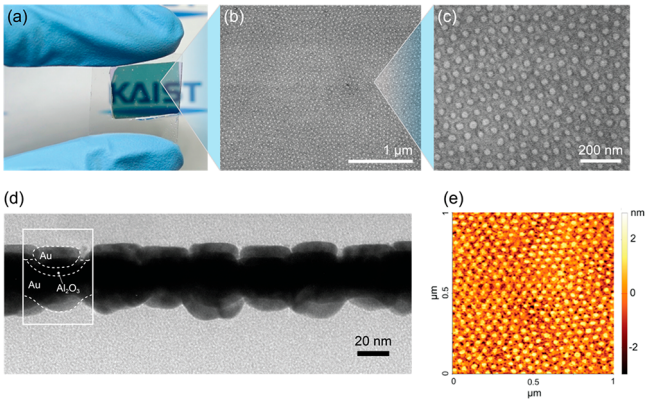

Figure 2. Optical and structural characteristics of nano−lotus pod metasurface. (a) Photograph of 5 nm gap nano−lotus pod structure with a size of over 1 cm^2. (b, c) SEM images of the 5 nm gap nano−lotus pod structure with different magnifications. The scale bars are included in the image. (d) HRTEM image of the Al_2O_3 5 nm gap nano−lotus pod structure in cross-sectional view. (e) AFM image of the sample.

https://doi.org/10.1021/acsphotonics.0c01882
ACS Photonics XXXX, XXX, XXX−XXX

unit structures are distributed densely (in a deep-subwavelength period) and uniformly so that the scattering is canceled in any nonspecular direction. If distributed in a larger period or nonuniformly, the film would exhibit strong angular scattering, becoming diffracting or translucent. Figure 2b and c are scanning electron microscopy (SEM) images of the nano−lotus pod structure from the top, viewed at different magnifications. In Figure 2d, the high-resolution transmission electron microscopy (HRTEM) image shows a cross-sectional view of the sample with a 5 nm thick Al_2O_3 gap. The SEM and HRTEM images agree with our schematics in Figure 1.

Due to their exposure to elevated temperature during the ALD process, the final shape of the gold nanodots deviates from a perfect hemisphere and resembles a truncated oblate spheroid. Since the shape of the gold nanodots has a critical impact on the resonance wavelength, the structural parameters from the HRTEM images were taken into account during the analysis of the mode profiles with numerical simulations. The morphology data taken from AFM (Figure 2e) also confirms the quality of the sample, with minimal surface roughness, comparable to previous template stripping studies.[31] The 5 nm height difference between the gold dots and the continuous gold layer corresponds to the Al_2O_3 deposition thickness, and could be potentially avoided by a careful pre-etching of the substrate by the same amount before ALD if required.

Figure 3a illustrates how we can understand the optical resonance of the nano−lotus pod structure starting from a

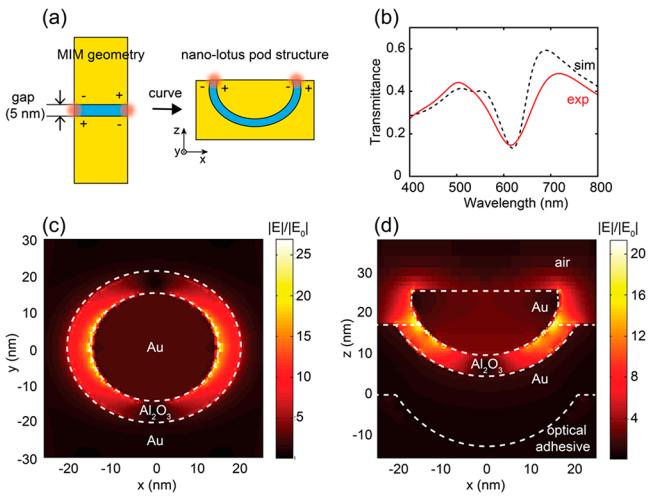

Figure 3. Optical analysis of nano−lotus pods. (a) Schematic of nano−lotus pod structure compared to MIM waveguide geometry. (b) Experimental (red, solid line) and calculated (black, dashed line) transmission spectra of nano−lotus pod array. (c, d) Calculated electric field amplitude profile in top view (c) and cross-sectional view (d).

simple MIM waveguide. Our nanoresonator can be considered as a truncated MIM waveguide structure that is bent to a hemispherical shape to expose both of its two open end faces, at which the maximum electric field intensity occurs, to the same surface (Figures 3a and S3 in the Supporting Information). Based on our understanding on the MIM resonator, we can judiciously design the resonance wavelength by changing the geometrical parameters of the resonator. With the sub-100 nm dimension of the unit resonator, it is possible to design such structure capable of confining visible lights in a small volume. As light−matter interactions are directly proportional to the local strength of electric fields, these exposed faces help harnessing the strong optical resonance to various visible wavelength light applications including surface-enhanced Raman scattering (SERS) and nonlinear optics. Additionally, being atomically flat and uniform, the proposed structure can be utilized as an effective SERS substrate even for very thin, stiff, and flat analytes such as two-dimensional (2D) semiconductors.

To analyze the resonance and light localization properties of our proposed nanostructures quantitatively, first-principle numerical simulations were performed based on the finite-difference time-domain (FDTD) method, in addition to experimental characterizations. Figure 3b shows the simulated (dashed line) and experimentally measured (solid line) transmittance spectra, which closely resemble each other. Most importantly, transmittance dip wavelengths correspond to each other, indicating that the resonant mode predicted by simulation is consistent with the experimental results. Transmittance drops for the resonance wavelength, signaling that light energy is resonantly excited at the nanostructure with the quality factor of 12.4 for numerical simulation result and 7.25 for experimental result, respectively. Simulated reflection and absorption spectra can be found in Figure S4 in the Supporting Information. The degree of electric field confinement in the nanogap region can be found in the electric field intensity profiles as well as in the calculated mode volume. The effective mode volume (V_m) is defined as

$$V_m = \frac{\iiint W(r)\mathrm{d}^3 r}{\max[W(r)]} \quad (1)$$

where $W(r)$ is the local electromagnetic energy density calculated based on a multiple Drude-Lorentz oscillator model, which is more accurate than a commonly used expression based only on the first differential of the permittivity as a function of frequency.[32−34] Using this definition, the calculated effective mode volume of the nano−lotus pod was $1.57 \times 10^{-5}\lambda_0^3$.

The associated electric field profiles on resonance are presented in Figure 3c,d, which shows an increase in the maximum field amplitude of 21 over that of the incident plane wave. It is obvious that the electric field is most enhanced near the sample surface. This is congruent with the typical electric field profile inside an open-end waveguide cavity (Figure S3 in the Supporting Information).[9] When the gap is gradually decreased from 5 to 1.5 nm, the maximum field as well as resonant wavelength increase monotonically, denoting high field localization and optical tunability of these resonators (Figure S5 in the Supporting Information). If necessary, the field enhancement and the resonant wavelength can be separately controlled by varying the diameter of gold nanodots, while utilizing block copolymers with different molecular weights (Figure S6 in the Supporting Information).

For experimental confirmation of the enhanced electric fields, SERS measurements were performed. Most plasmonic SERS substrate research so far has focused on making embossed and often random structures to induce field enhancement.[35] By contrast, our sample possesses an intensity and wavelength controllable optical resonance while preserving an atomically flat surface. Moreover, the electric hot spots are exposed on the surface and densely arranged in a regular periodic fashion, effectively forming an optically uniform metasurface. This makes it potentially ideal as a universal SERS

https://doi.org/10.1021/acsphotonics.0c01882
ACS Photonics XXXX, XXX, XXX−XXX

substrate. Especially, it can be utilized for very thin analytes such as hexagonal boron-nitride, graphene, or graphene oxides. Flat substrates are also beneficial in Raman fingerprint analysis of substances like thiol self-assembled monolayer groups, whose Raman peaks are influenced by substrate flatness.[36]

We chose graphene oxide, whose Raman fingerprint is well-known, as a typical 2D analyte example.[37,38] Figure 4a presents

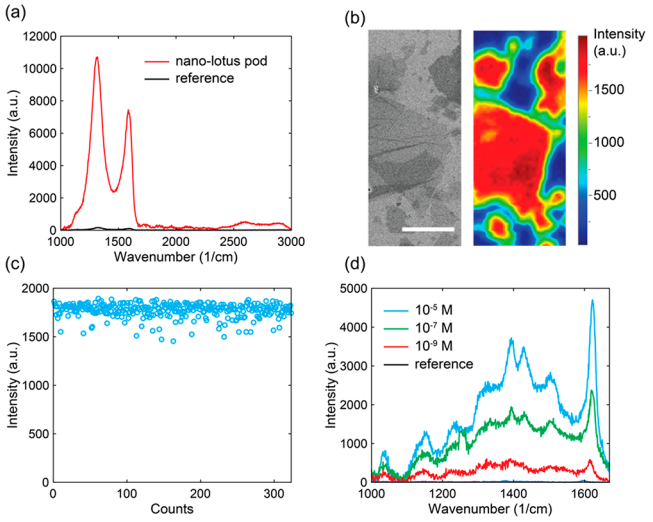

Figure 4. Nano–lotus pod metasurface as a SERS platform. (a) Raman spectra of a single graphene oxide layer on the 5 nm gap nano–lotus pod structure compared to that on the gold thin film. (b) SEM image and corresponding Raman imaging of a single graphene oxide layer on a 5 nm gap nano–lotus pod structure (scale bar represents 5 μm). (c) Raman signal distribution of 323 points in graphene oxide on a 5 nm gap nano–lotus pod structure sample. Standard deviation was 4.24%. (d) Raman signal spectra of methylene blue solution with various concentrations (10^{-5}, 10^{-7}, and 10^{-9} M) on the nano–lotus pod structure and reference data of 10^{-3} M methylene blue solution on a flat gold substrate.

the Raman signal intensity spectra of monolayer graphene oxide on the sample and on a bare flat gold substrate for comparison. A pump laser emitting at a 633 nm wavelength, which coincides with the resonance of the nano–lotus pod structure, was used to excite the graphene oxide on both samples. The main peaks of the graphene oxide, 1320 cm^{-1} (D-band) and 1585 cm^{-1} (G-band), are clearly observed in both spectra. Considering that bulk 2D materials have different material properties than the single layer, we calculated enhancement factor (EF) for the 2D planar analyte using normalized Raman enhancement (NRE) rather than using conventional SERS EF which assumes scattering volume for non-SERS measurement.[39,40] NRE is estimated to be 64 for D-band peak of graphene oxide, which demonstrates enhanced sensing performance for flat planar analytes than previous works.[40,41] However, in the current structure, the position of the maximum electric field location is slightly recessed due to the height difference of the gold dot and the gold matrix. It is possible to improve NRE further by fabricating the ultraflat surface with pre-etching the silicon substrate as mentioned before.

The nano–lotus pod structure array may serve as a good light–matter interaction platform for several reasons. First, the resonance can be spectrally tuned by controlling the thickness of the gap, by changing the gap material, or by varying the nanodot diameter. In addition to the significant enhancement of interaction, the nano–lotus pod structure array guarantees high uniformity throughout the entire sample. The uniformity of the sample is demonstrated in Figure 4b, showing a SEM image and Raman mapping of monolayer graphene oxide. Within the area of monolayer graphene oxide, the Raman signals show nearly constant intensity. In the region where two graphene oxide flakes overlap, the Raman signal increases but not as much as double the value of a monolayer flake, confirming that the enhancement is strongly confined to the surface. Evaluation of 323 SERS spectra on a specific flake of graphene oxide indicates an average SERS intensity of 1766 counts with a normalized standard deviation of 4.24%, as shown in Figure 4c. This very low standard deviation shows the uniformity of our nano–lotus pod structure and the consistency of the enhancement effect. This uniformity continues to other flakes on a different part of the sample, showing congruent behavior over the large sample area (Figure S7 in the Supporting Information). Also, to demonstrate the nano–lotus pod structure can be used for detecting not only 2D materials but also typical Raman analytes, Raman signals of methylene blue are demonstrated in Figure 4d. As the concentration of methylene blue decreases from 10^{-5} M to 10^{-9} M, Raman peaks are clearly detectable including the main peak of methylene blue at 1620 cm^{-1}.[42] Even at a very low concentration of 10^{-9} M, this methylene blue peak is detectable, while the Raman signal from the 10^{-3} M methylene blue solution on the flat gold substrate is very low.

In summary, a plasmonic nano–lotus pod structure array having a strong resonance in the visible range was proposed and fabricated for the first time using block copolymer self-assembly combined with atomic layer deposition and template stripping. The sub-100 nm feature size of the resonator, required for visible wavelength resonance, and its uniformity over a large area are not readily accessible by conventional lithography, and here they were accomplished without any delicate and time-consuming lithographic step. We calculated that the three-dimensional nano–lotus pod has an extreme confinement of visible light into a mode volume of $1.57 \times 10^{-5}\lambda_0^3$ as a waveguide-based cavity. The resonance behavior was confirmed using simulated and experimental transmittance measurements, which correlated with each other. The electric field is focused largely on the ultraflat surface of the nano–lotus pod structure, and this advantage was used to demonstrate the enhancement of Raman signal for a 2D analyte with high uniformity. We believe that this nano–lotus pod design and the method of fabricating uniform nanogap features in a large scale can open new opportunities for studying strong light–matter interactions in visible wavelengths and for the applications in sensing and communications.

EXPERIMENTAL SECTION

Preparation of the PS-*b*-PMMA Block Copolymer Template. A PS-*r*-PMMA copolymer brush layer was spin-coated onto a cleaned silicon wafer, for the surface neutralization. After a thermal annealing at 160 °C for over 12 h in vacuum, the unreacted PS-*r*-PMMA was rinsed with toluene. The PS-*b*-PMMA block copolymer (M_n of 140 kg mol^{-1} and 65 kg mol^{-1} for each of the PS and PMMA blocks) was dissolved in toluene and spin coated to create a thin film of 80 nm thickness. The sample was thermally annealed at 250 °C for 6 h in vacuum, then cross-linked to selectively degrade the

https://doi.org/10.1021/acsphotonics.0c01882
ACS Photonics XXXX, XXX, XXX–XXX

PMMA cylinder domains. After wet etching, the PMMA was selectively removed, leaving a PS matrix with perforated cylinder holes with a diameter of 30 nm. For thorough removal of PMMA, reactive ion etching with O_2 plasma was additionally conducted for 10 s.

Atomic Layer Deposition Method. Trimethyl aluminum (TMA) and H_2O were used as the aluminum and oxidation sources, respectively. For the ALD process, TMA was sourced first, and purged with inert argon (Ar) gas. For the oxidation, H_2O was sourced and also purged with Ar gas. After repeating this cycle 36 times at 300 °C, a 5 nm thick film of Al_2O_3 was obtained.

Preparation of Raman Analyte. For the Raman analysis, graphene oxide was synthesized following the modified Hummer's method.[43] The graphene oxide concentration was diluted sufficiently so that monolayer graphene oxide flakes could be identified for Raman analysis after spin-coating on both the substrate with nano−lotus pod structure array and a bare gold substrate, used as a reference.

Structural Characterization. SEM images after template stripping were obtained from a Hitachi S-4800 SEM with a low accelerating voltage of 3 kV to avoid charging of the sample. HRTEM images were obtained using a Tecnai TF30 ST which is a field emission transmission electron microscope from FEI Company, with an accelerating voltage of 300 kV. A focused ion beam using Helios Nanolab 4550 F1 from FEI Company was used to fabricate HRTEM specimens for observation of the cross-sectional view of the sample. For AFM measurements, a XE-100 from Park Systems in noncontact mode was used with a scan rate of 0.7 Hz. UV/visible spectra were measured by a PerkinElmer Lambda 1050 UV/vis/NIR spectrophotometer with a reference sample of the glass substrate.

Raman Measurement. Raman signals were detected using a Labram Aramis Jobin Yvon Horiba microRaman system with He−Ne 633 nm laser with excitation power of 10 mW. Data were collected using gratings of 600 g mm^{-1} and an ×50 objective lens with a long working distance, for 10 s to avoid damage of the graphene oxide. Different concentration of methylene blue solution with methanol at 10 μL in volume is deposited on the nano−lotus pod structure array as well as flat gold substrate (reference). Data were collected for 10 s.

Numerical Simulations. To verify electric field enhancement and transmission spectra theoretically, full-field 3D simulations with finite-difference time-domain (FDTD) method from Lumerical were adopted. Nano−lotus pods are periodically arranged in a hexagonal lattice, with the nearest distance between two resonators set as 60 nm. For simulations, we instead used rectangular unit cell including two nano−lotus pods. We used the periodic boundaries on both x and y directions and perfectly matched layers on both z directions. Gold nanodots with rounded corners are assumed. Plane wave with normal incidence is illuminated in the z direction, and the electric field is polarized along the x direction. The refractive index of ALD-grown Al_2O_3 was kept constant as 1.5.

Characteristic Volume Calculations. *Unit Volume Calculation.* From the top, unit nano−lotus pods are periodically arranged in a hexagonal lattice with the nearest distance (a) between two resonators being 60 nm. In here, for convenience, we set the primitive lattice to be rectangle ($a \times \frac{\sqrt{3}}{2}a$, a = 60 nm). For the thickness, maximum height of a resonator consisting of two gold domains (15 and 20 nm thick) and nanogap (5 nm thick) in between is 40 nm. Therefore, we defined the unit volume as $52 \times 60 \times 40$ nm^3, as illustrated in Figure 1.

Effective Mode Volume and Quality Factor Calculation. Effective mode volume is calculated using the eq 1 in the main text. Modal energy distributions are obtained by using apodization in the discrete Fourier transform monitors in FDTD simulation. Quality factors are estimated through fitting the measured and simulated spectra to Lorentzian functions.

■ ASSOCIATED CONTENT

Supporting Information

The Supporting Information is available free of charge at https://pubs.acs.org/doi/10.1021/acsphotonics.0c01882.

Optical simulations, photographs of the sample, AFM image of the silicon wafer after template stripping, additional Raman intensity mapping, and SEM of the corresponding area (PDF)

■ AUTHOR INFORMATION

Corresponding Author

Jonghwa Shin − *Department of Materials Science and Engineering, Korea Advanced Institute of Science and Technology, Daejeon 34141, Republic of Korea;* orcid.org/0000-0003-0712-464X; Email: qubit@kaist.ac.kr

Authors

Nayeun Lee − *Geballe Laboratory for Advanced Materials, Stanford University, Stanford, California 94305, United States;* orcid.org/0000-0002-9633-8000

Reehyang Kim − *Department of Materials Science and Engineering, Korea Advanced Institute of Science and Technology, Daejeon 34141, Republic of Korea;* orcid.org/0000-0002-7643-5604

Ju Young Kim − *Electronics and Telecommunications Research Institute, Daejeon 34129, Republic of Korea;* orcid.org/0000-0002-2396-4457

Jong Beom Ko − *Department of Materials Science and Engineering, Korea Advanced Institute of Science and Technology, Daejeon 34141, Republic of Korea*

Sang-Hee Ko Park − *Department of Materials Science and Engineering, Korea Advanced Institute of Science and Technology, Daejeon 34141, Republic of Korea;* orcid.org/0000-0001-7165-8211

Sang Ouk Kim − *Department of Materials Science and Engineering, Korea Advanced Institute of Science and Technology, Daejeon 34141, Republic of Korea;* orcid.org/0000-0003-1513-6042

Mark L. Brongersma − *Geballe Laboratory for Advanced Materials, Stanford University, Stanford, California 94305, United States;* orcid.org/0000-0003-1777-8970

Complete contact information is available at: https://pubs.acs.org/10.1021/acsphotonics.0c01882

Notes

The authors declare no competing financial interest.

■ ACKNOWLEDGMENTS

This work was supported by the National Research Foundation of Korea (NRF) Grant funded by the Korea government (MSIT; Nos. 2018M3D1A1058998,

2018R1A2A3075518, 2021R1A2C200868711, and 2013M3A6B1078874 (the Hybrid Interface Materials Research Group)) and by the Department of Energy Grant funded by the United States government (No. DE-FG07-ER46426).

REFERENCES

(1) Schuller, J. A.; Barnard, E. S.; Cai, W.; Jun, Y. C.; White, J. S.; Brongersma, M. L. Plasmonics for Extreme Light Concentration and Manipulation. *Nat. Mater.* **2010**, *9* (3), 193−204.
(2) Stockman, M. I. Nanofocusing of Optical Energy in Tapered Plasmonic Waveguides. *Phys. Rev. Lett.* **2004**, *93* (13), 137404.
(3) Koenderink, A. F.; Alu, A.; Polman, A. Nanophotonics: Shrinking Light-Based Technology. *Science* **2015**, *348* (6234), 516−521.
(4) Liu, N.; Tang, M. L.; Hentschel, M.; Giessen, H.; Alivisatos, A. P. Nanoantenna-Enhanced Gas Sensing in a Single Tailored Nanofocus. *Nat. Mater.* **2011**, *10* (8), 631−636.
(5) Kinkhabwala, A.; Yu, Z.; Fan, S.; Avlasevich, Y.; Müllen, K.; Moerner, W. E. Large Single-Molecule Fluorescence Enhancements Produced by a Bowtie Nanoantenna. *Nat. Photonics* **2009**, *3* (11), 654−657.
(6) Russell, K. J.; Liu, T. L.; Cui, S.; Hu, E. L. Large Spontaneous Emission Enhancement in Plasmonic Nanocavities. *Nat. Photonics* **2012**, *6* (7), 459−462.
(7) Luo, Y.; Shepard, G. D.; Ardelean, J. V.; Rhodes, D. A.; Kim, B.; Barmak, K.; Hone, J. C.; Strauf, S. Deterministic Coupling of Site-Controlled Quantum Emitters in Monolayer WSe2 to Plasmonic Nanocavities. *Nat. Nanotechnol.* **2018**, *13* (12), 1137−1142.
(8) Kleemann, M. E.; Chikkaraddy, R.; Alexeev, E. M.; Kos, D.; Carnegie, C.; Deacon, W.; De Pury, A. C.; Große, C.; De Nijs, B.; Mertens, J.; Tartakovskii, A. I.; Baumberg, J. J. Strong-Coupling of WSe_2 in Ultracompact Plasmonic Nanocavities at Room Temperature. *Nat. Commun.* **2017**, *8* (1), na.
(9) Miyazaki, H. T.; Kurokawa, Y. Squeezing Visible Light Waves into a 3-Nm-Thick and 55-Nm-Long Plasmon Cavity. *Phys. Rev. Lett.* **2006**, *96* (9), 097401.
(10) Kuttge, M.; García De Abajo, F. J.; Polman, A. Ultrasmall Mode Volume Plasmonic Nanodisk Resonators. *Nano Lett.* **2010**, *10* (5), 1537−1541.
(11) Chikkaraddy, R.; De Nijs, B.; Benz, F.; Barrow, S. J.; Scherman, O. A.; Rosta, E.; Demetriadou, A.; Fox, P.; Hess, O.; Baumberg, J. J. Single-Molecule Strong Coupling at Room Temperature in Plasmonic Nanocavities. *Nature* **2016**, *535* (7610), 127−130.
(12) Kim, M. K.; Sim, H.; Yoon, S. J.; Gong, S. H.; Ahn, C. W.; Cho, Y. H.; Lee, Y. H. Squeezing Photons into a Point-Like Space. *Nano Lett.* **2015**, *15* (6), 4102−4107.
(13) Suh, J. Y.; Kim, C. H.; Zhou, W.; Huntington, M. D.; Co, D. T.; Wasielewski, M. R.; Odom, T. W. Plasmonic Bowtie Nanolaser Arrays. *Nano Lett.* **2012**, *12* (11), 5769−5774.
(14) Li, Z.; Kou, J. L.; Kim, M.; Lee, J. O.; Choo, H. Highly Efficient and Tailorable On-Chip Metal-Insulator-Metal Plasmonic Nanofocusing Cavity. *ACS Photonics* **2014**, *1* (10), 944−953.
(15) Siddique, R. H.; Kumar, S.; Narasimhan, V.; Kwon, H.; Choo, H. Aluminum Metasurface with Hybrid Multipolar Plasmons for 1000-Fold Broadband Visible Fluorescence Enhancement and Multiplexed Biosensing. *ACS Nano* **2019**, *13* (12), 13775−13783.
(16) Tian, C.; Deng, Y.; Zhao, D.; Fang, J. Plasmonic Silver Supercrystals with Ultrasmall Nanogaps for Ultrasensitive SERS-Based Molecule Detection. *Adv. Opt. Mater.* **2015**, *3* (3), 404−411.
(17) Wang, L.; Uppuluri, S. M.; Jin, E. X.; Xu, X. Nanolithography Using High Transmission Nanoscale Bowtie Apertures. *Nano Lett.* **2006**, *6* (3), 361−364.
(18) Haynes, C. L.; Van Duyne, R. P. Nanosphere Lithography: A Versatile Nanofabrication Tool for Studies of Size-Dependent Nanoparticle Optics. *J. Phys. Chem. B* **2001**, *105* (24), 5599−5611.
(19) Wang, H.; Levin, C. S.; Halas, N. J. Nanosphere Arrays with Controlled Sub-10-Nm Gaps as Surface-Enhanced Raman Spectroscopy Substrates. *J. Am. Chem. Soc.* **2005**, *127* (43), 14992−14993.
(20) Im, H.; Bantz, K. C.; Lee, S. H.; Johnson, T. W.; Haynes, C. L.; Oh, S.-H. Self-Assembled Plasmonic Nanoring Cavity Arrays for SERS and LSPR Biosensing. *Adv. Mater.* **2013**, *25* (19), 2678−2685.
(21) Yang, Y.; Gu, C.; Li, J. Sub-5 Nm Metal Nanogaps: Physical Properties, Fabrication Methods, and Device Applications. *Small* **2019**, *15* (5), 1804177.
(22) Bahk, Y.-M.; Kim, D.-S.; Park, H.-R. Large-Area Metal Gaps and Their Optical Applications. *Adv. Opt. Mater.* **2019**, *7* (1), 1800426.
(23) Akselrod, G. M.; Huang, J.; Hoang, T. B.; Bowen, P. T.; Su, L.; Smith, D. R.; Mikkelsen, M. H. Large-Area Metasurface Perfect Absorbers from Visible to Near-Infrared. *Adv. Mater.* **2015**, *27* (48), 8028−8034.
(24) Chen, X.; Park, H. R.; Pelton, M.; Piao, X.; Lindquist, N. C.; Im, H.; Kim, Y. J.; Ahn, J. S.; Ahn, K. J.; Park, N.; Kim, D. S.; Oh, S. H. Atomic Layer Lithography of Wafer-Scale Nanogap Arrays for Extreme Confinement of Electromagnetic Waves. *Nat. Commun.* **2013**, *4* (1), 2361−17.
(25) Chen, X.; Ciracì, C.; Smith, D. R.; Oh, S.-H. Nanogap-Enhanced Infrared Spectroscopy with Template-Stripped Wafer-Scale Arrays of Buried Plasmonic Cavities. *Nano Lett.* **2015**, *15* (1), 107−113.
(26) Leibler, L. Theory of Microphase Separation in Block Copolymers. *Macromolecules* **1980**, *13* (6), 1602−1617.
(27) Ruiz, R.; Kang, H.; Detcheverry, F. A.; Dobisz, E.; Kercher, D. S.; Albrecht, T. R.; De Pablo, J. J.; Nealey, P. F. Density Multiplication and Improved Lithography by Directed Block Copolymer Assembly. *Science* **2008**, *321* (5891), 936−939.
(28) Li, T.; Wu, K.; Rindzevicius, T.; Wang, Z.; Schulte, L.; Schmidt, M. S.; Boisen, A.; Ndoni, S. Wafer-Scale Nanopillars Derived from Block Copolymer Lithography for Surface-Enhanced Raman Spectroscopy. *ACS Appl. Mater. Interfaces* **2016**, *8* (24), 15668−15675.
(29) Shin, D. O.; Jeong, J. R.; Han, T. H.; Koo, C. M.; Park, H. J.; Lim, Y. T.; Kim, S. O. A Plasmonic Biosensor Array by Block Copolymer Lithography. *J. Mater. Chem.* **2010**, *20* (34), 7241−7247.
(30) Park, H.-R.; Namgung, S.; Chen, X.; Lindquist, N. C.; Giannini, V.; Francescato, Y.; Maier, S. A.; Oh, S.-H. Perfect Extinction of Terahertz Waves in Monolayer Graphene over 2-Nm-Wide Metallic Apertures. *Adv. Opt. Mater.* **2015**, *3* (5), 667−673.
(31) Nagpal, P.; Lindquist, N. C.; Oh, S. H.; Norris, D. J. Ultrasmooth Patterned Metals for Plasmonics and Metamaterials. *Science* **2009**, *325* (5940), 594−597.
(32) Ruppin, R. Electromagnetic Energy Density in a Dispersive and Absorptive Material. *Phys. Lett. A* **2002**, *299* (2−3), 309−312.
(33) Nunes, F. D.; Borges, B.-H. V.; Weiner, J. Analysis of Dispersive and Dissipative Media with Optical Resonances. *Opt. Express* **2012**, *20* (14), 15679.
(34) Rakić, A. D.; Djurišić, A. B.; Elazar, J. M.; Majewski, M. L. Optical Properties of Metallic Films for Vertical-Cavity Optoelectronic Devices. *Appl. Opt.* **1998**, *37* (22), 5271.
(35) Karthick Kannan, P.; Shankar, P.; Blackman, C.; Chung, C. Recent Advances in 2D Inorganic Nanomaterials for SERS Sensing. *Adv. Mater.* **2019**, *31* (34), 1803432.
(36) Bryant, M. A.; Pemberton, J. E. Surface Raman Scattering of Self-Assembled Monolayers Formed from 1-Alkanethiols: Behavior of Films at Au and Comparison to Films at Ag. *J. Am. Chem. Soc.* **1991**, *113* (22), 8284−8293.
(37) Fan, W.; Lee, Y. H.; Pedireddy, S.; Zhang, Q.; Liu, T.; Ling, X. Y. Graphene Oxide and Shape-Controlled Silver Nanoparticle Hybrids for Ultrasensitive Single-Particle Surface-Enhanced Raman Scattering (SERS) Sensing. *Nanoscale* **2014**, *6* (9), 4843−4851.
(38) Jiang, G.; Lin, Z.; Chen, C.; Zhu, L.; Chang, Q.; Wang, N.; Wei, W.; Tang, H. TiO2 Nanoparticles Assembled on Graphene Oxide Nanosheets with High Photocatalytic Activity for Removal of Pollutants. *Carbon* **2011**, *49* (8), 2693−2701.

https://doi.org/10.1021/acsphotonics.0c01882
ACS Photonics XXXX, XXX, XXX−XXX

(39) Le Ru, E. C.; Blackie, E.; Meyer, M.; Etchegoin, P. G. Surface Enhanced Raman Scattering Enhancement Factors: A Comprehensive Study. *J. Phys. Chem. C* **2007**, *111* (37), 13794−13803.
(40) Thareja, V.; Esfandyarpour, M.; Kik, P. G.; Brongersma, M. L. Anisotropic Metasurfaces as Tunable SERS Substrates for 2D Materials. *ACS Photonics* **2019**, *6* (8), 1996−2004.
(41) Cai, H.; Meng, Q.; Zhao, H.; Li, M.; Dai, Y.; Lin, Y.; Ding, H.; Pan, N.; Tian, Y.; Luo, Y.; Wang, X. High-Throughput Fabrication of Ultradense Annular Nanogap Arrays for Plasmon-Enhanced Spectroscopy. *ACS Appl. Mater. Interfaces* **2018**, *10* (23), 20189−20195.
(42) Merlen, A.; Gadenne, V.; Romann, J.; Chevallier, V.; Patrone, L.; Valmalette, J. C. Surface Enhanced Raman Spectroscopy of Organic Molecules Deposited on Gold Sputtered Substrates. *Nanotechnology* **2009**, *20* (21), 215705.
(43) Kim, J. E.; Han, T. H.; Lee, S. H.; Kim, J. Y.; Ahn, C. W.; Yun, J. M.; Kim, S. O. Graphene Oxide Liquid Crystals. *Angew. Chem., Int. Ed.* **2011**, *50* (13), 3043−3047.

https://doi.org/10.1021/acsphotonics.0c01882
ACS Photonics XXXX, XXX, XXX−XXX